

SINERGI Vol. 29, No. 3, October 2025: 833-844 http://publikasi.mercubuana.ac.id/index.php/sinergi http://doi.org/10.22441/sinergi.2025.3.023



An FFT-based vibration characterization of the road profile of a two-wheeler electric vehicle



Mohamad Ardy Firmansyah*^{1,5}, Dafit Feriyanto¹, Himma Firdaus^{2,3}, Hadi Pranoto¹, Istiqomah^{4,5}

- ¹Department of Mechanical Engineering, Faculty of Engineering, Universitas Mercu Buana
- ²Research Center for Electrical Technology, National Research and Innovation Agencies (BRIN), Indonesia.
- ³Electrical Engineering Department, Universitas Pamulang, Indonesia.
- ⁴Mechanical Engineering Department, President University, Indonesia.
- ⁵Vehicle Testing and Certification Center, Ministry of Transportation, Indonesia.

Abstract

Vibration is an inevitable physical phenomenon; excessive and uncontrolled amounts of vibration can result in damage and system failure. In accordance with various automotive product certification standards, vehicle batteries or rechargeable electrical energy storage systems (REESS) must undergo a vibration test to assess their mechanical integrity. This study aims to broaden the perspective on vibration assessment by examining it during vehicle operation and assessing the protective capabilities of vehicle suspension against vibrations from damaged roads in two-wheeled electric motor vehicles. The proposed method involves installing an accelerometer on the battery pack body, which is placed in the battery compartment. The experimental setup involved conducting tests on a 125-meter track, with the vehicle traversing roads characterized by concrete cracks, uneven surfaces, and potholes. Two distinct speed variations were selected for analysis: 10 and 15 kilometers per hour. The results obtained from the Rion VA 12 portable vibration analyzer are presented as a plot of the fast Fourier transform (FFT) graph. The maximum acceleration recorded was 2.35 and 1.98 G at the same frequency of 7 hertz (Hz). This research method and result align with others, including those focused on assessing road damage, passenger comfort, and vehicle component damage, such as shock absorbers. In the future, the development of a vehicle battery support structure is anticipated to further minimize vibration disturbance by reducing the peak acceleration values depicted in the FFT graph. The minimization of incoming vibrations is expected to enhance the safety and durability of the battery pack.

This is an open-access article under the CC BY-SA license.



Keywords:

Fast Fourier Transformation; REESS; Vibration;

Article History:

Received: January 20, 2025 Revised: March 25 2025 Accepted: April 18, 2025 Published: September 5, 2025

Corresponding Author:

Mohamad Ardy Firmansyah Mechanical Engineering Department, Universitas Mercu Buana, Indonesia Email: mohamad_ardy@dephub.go.id

INTRODUCTION

Vibration is the physical phenomenon showing a rotational or translational motion in a structure. It is widely accepted that excessive vibration can have a detrimental impact on a structure. Vibration is also frequently linked with the deterioration of machinery or structural components [1][2]. In the field of vehicle dynamics,

vibration is a highly regarded factor. It is important to note that its significance extends to several key areas, including passenger comfort, maintenance, prediction of the lifespan of vehicle components, and vehicle design itself [3].

One frequently employed analytical technique in the domain of vibration is the fast Fourier transformation (FFT). The FFT represents

a more practical and expedient transformation than the Discrete Fourier transform (DFT) [4][5]. The analysis of waves and vibrations is typically expressed in the frequency domain, whereas the data obtained from experimental vibration measurements are generally represented in the time domain. The FFT facilitates the straightforward identification of the dominant frequency at which the most substantial vibration magnitude occurs [6].

Vibration research in electric vehicles is frequently concentrated on battery cells. This implies that the battery cell is the element directly exposed to vibrations [1, 7, 8, 9, 10]. While this assertion is not entirely inaccurate, it is also not precise. During operation, the electric vehicle battery is not directly influenced by vibration. However, if we trace the vibration from the component with the narrowest profile, it becomes evident that numerous components can mitigate the electric vehicle battery's vibration. These components include the battery holder, elastic foundation, battery pack, and vehicle suspension, all of which contribute to reducing the overall vibration [11].

A substantial body of prior research has addressed the topic of vehicle vibrations, examining the phenomenon in the context of various types of tracks, including those that are conditioned, highway, and off-road. The following paragraphs will endeavor to elucidate this matter. A study has identified a method for predicting vibration testing outcomes without the necessity of collecting data directly in the field. The method entails the integration of road and vehicle PSD functions with additional variables, including road roughness, vehicle speed, and trip duration [12].

A study mapping the unevenness of runways at seven Chinese airports found that waviness and unevenness are interrelated. The study states that these two characteristics are closely correlated with the vibrations felt by aircraft bodies [13].

Another study mentioned that a road profile survey was conducted over a distance of 1,860 km using nine different types of cars. In the study, data were collected by installing accelerometers on the frame near the driver's seat and on the driver's seat surface. The PSD data was then extracted. This data collection method is used as a reference in the existing research. Similar to previous research, this study aims to characterize the levels of comfort, unevenness, and waviness caused by a vehicle ride [14].

As far as off-road is concerned, a study shows the transmissibility data between the frame of an agricultural tractor and the surface of a driver's seat with air suspension. A similar method was used in the previous section. The presence of and implementation reduced ballast transmissibility values in the longitudinal direction, while the pneumatic seat gave the driver's seat good transmissibility values in the vertical axis direction [15, 16, 17]. A potential method for vibration effects mitigating involves development of magnetorheological elastomer (MRE) materials. These materials are classified as dampers, characterized by their ability to modify stiffness through the strategic placement of electrically charged coils, which are subjected to a specific current [18].

In considering the impact of motor noise on passenger comfort, a study identified electromagnetic and gear-meshing noise as the primary sources of noise in electric vehicles. Experiments were conducted in an anechoic chamber to investigate this further, focusing solely on the traction motor and including speed variations. Additionally, simulations were performed to validate the findings [19].

From various previous studies, there is a lack of information on how the characteristics of electric vehicles are affected when they are directly exposed to vibration during road operation, especially on low-category roads such as categories C, D, and E, where vibration disturbances are certainly higher and more damaging. Vibration is also a mandatory item in the automotive product certification process, namely rechargeable energy storage system (REESS), which is included in various certification regulations such as UN ECE R136, ISO 18243, SNI 8872, FMVSS 305A, and other relevant standards.

In addition, this research builds on previous research that has discussed REESS testing in relation to battery packs [11]. The current research will examine the vibration aspect from a broader perspective, specifically the vibration of vehicles under operating conditions on roads with low pavement quality.

MATERIAL AND METHODS

The current research methodology involves documenting vibrations, with the primary objective of creating an FFT graph of a two-wheeled electric motorcycle. This was accomplished by conducting trials on roads characterized by substandard pavement quality. The subsequent descriptive paragraph outlines the procurement of the requisite tools and materials.

Material

The materials used in this research include the Gesits G1 electric motorcycle, shown in Figure 1, and the swappable battery pack, depicted in Figure 2. The specifications of the electric

motorcycle are as follows: Brand / Type: Gesits / G1 Curb weight: 94.5 kg Front tyre size: 80/80 R14 Rear tyre size: 100/80 R14

Front suspension type: Telescopic fork
Rear suspension type: Swing arm monoshock

L x W x H: 1,947 x 674 x 1,135 mm

Engine power: 2,000 watts Maximum speed: 70 km/h



Figure 1. Gesits G1



Figure 2. Gesits G1 Battery Pack

The OEM battery specifications employed

are as follows:

Number of Packs: 1 Pack Nominal Voltage: 72 VDC Nominal Capacity: 20 Ah Nominal Power: 1440 Wh Number of cells: 80 cells

Cell Configuration: 20 Series 4 Parallel

Nominal Cell Voltage: 3.6 VDC Nominal Cell Capacity: 5 Ah

Figure 2 shows a Rechargeable Electrical Energy Storage System (REESS) or battery pack utilized in this research. The battery is a type of swap battery that can be exchanged with another battery. It has an elongated shape with a handle at the top, allowing it to be removed easily [20][21]. The battery weighs 8.128 kg overall and has connectors at the top. The battery is placed in the battery compartment and held by the seat. The lower side of the battery pack is in direct contact with the battery compartment, while the upper side is in contact with the rubber retainer on the seat. This configuration ensures that the battery pack does not dislocate when the vehicle is in operation. Typically, no structure serves to reduce vibrations from the vehicle chassis to the battery pack.

The study utilized a portable vibration analyzer manufactured by Rion, designated as the VA 12 model. This instrument is frequently employed in both research and industrial settings for the purpose of analysing vibration, engine rotation, misalignment, and maintenance.



Figure 3. Rion VA 12

It offers an analysis of dimensional parameters, including displacement, speed, and acceleration [22]. The Rion VA 12 has been utilized in previous research and employed to assess passenger comfort levels in terms of seat adequate amplitude transmissibility (SEAT) [23]. SEAT is defined as the ratio of the vibration amplitude experienced by the passenger to the amplitude generated by the floor area. A comparable investigation was conducted using RION VM 54, a material that operates similarly to RION VA 12. The objective of this study was to ascertain the level of passenger comfort in a passenger car bench. The SEAT parameter was examined [24]. The Rion VA 12 model is depicted in Figure 3.

The following specifications pertain to the Rion VA 12 model:

Brand / Type: Rion VA 12

Accelerometer Type: Piezoelectric Window Function: Hanning Function

Frequency Measurement Range: 1 – 20 kHz Acceleration Measurement Range: 0.02 – 141.4 m/s²

Frequency span: 100 Hz, 200 Hz, 500 Hz, 1 kHz, 2 kHz, 5 kHz, 10 kHz, 20 kHz.

In order to mount the accelerometer on the REESS, a mounting apparatus is required. This mounting apparatus is manufactured using a 3D printing process. The accelerometer is attached to the REESS body by adjusting the slot design and reinforcing it with glue tack. It ensures that the position of the mount and the accelerometer do not shift during data collection. The design of the mounting apparatus and the 3D printing process are shown in Figure 4.

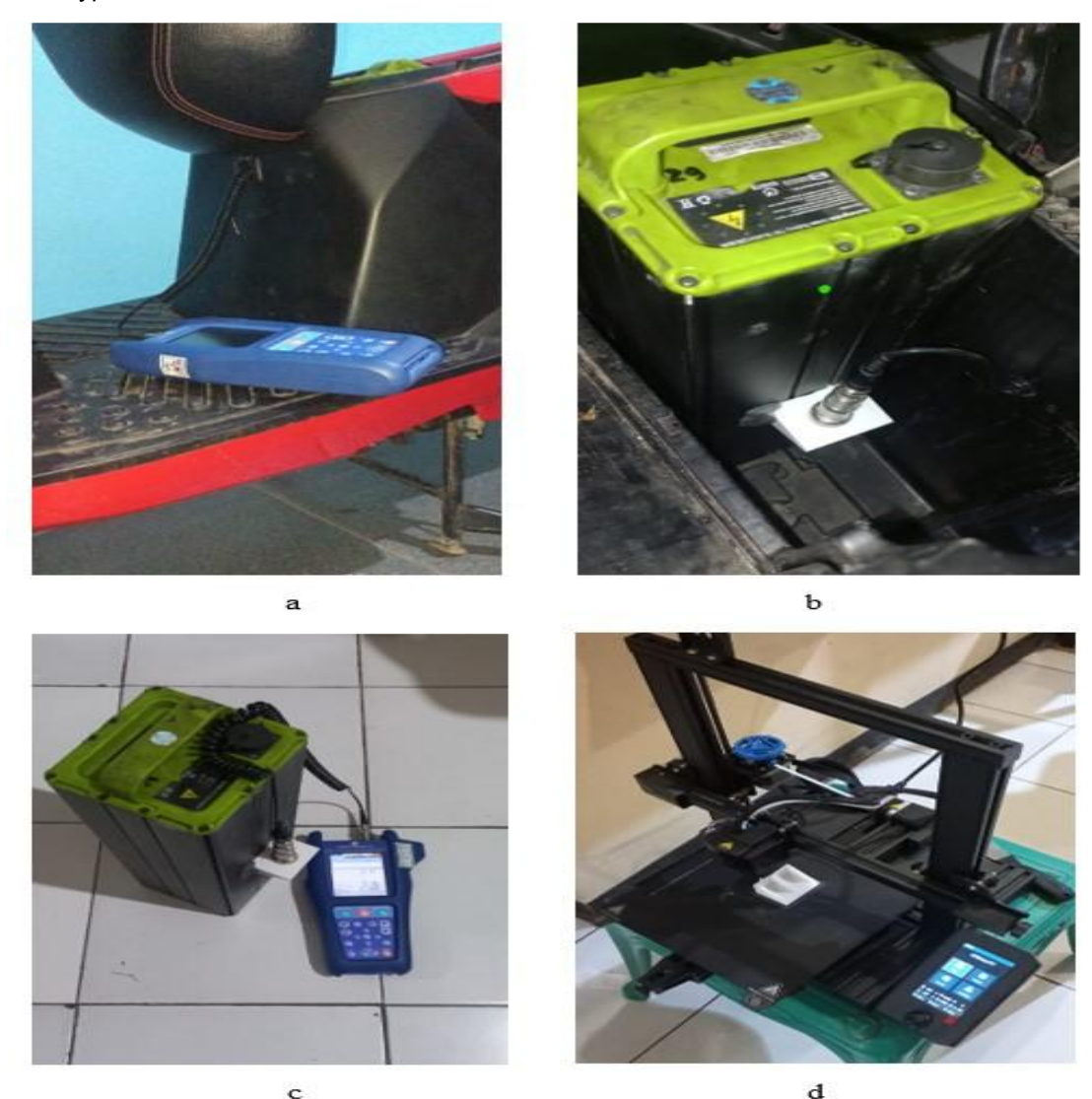


Figure 4. (a) Set up of the Rion VA 12 in the test vehicle, (b) Set up of the accelerometer in the vehicle battery, (c) Set up of the accelerometer when not installed, (d) Production of the accelerometer mounting by 3D printing.

Methods

The experimental trials were conducted on on-road sections exhibiting substandard pavement quality. The study selected a 125-metre track in Bekasi Regency, West Java Province, where most of the pavement is damaged, including uneven surfaces, cracked concrete, and road holes. The selected road characteristics represent low-grade roads (classes B and C) in accordance with ISO 8608. In such conditions, the operational speeds of vehicles are constrained due to the substantial vibrational disturbance caused by the low road grade [13][25].

The location of the selected GPS track is illustrated in Figure 5. Figure 6 illustrates the road conditions and the types of damage present. The test setup is initiated after compiling information about the tools and materials. The setup of the testing tools and materials is delineated in Figure 4, and vibration data is subsequently collected directly on the road at two speed variations: 10 km/h and 15 km/h. These speeds are deemed to be safe for the collection of vibration data. It is anticipated that increasing the speed beyond these levels may lead to accidents or cause damage to the specimen or the apparatus.

The Rion VA 12 is set at a frequency range of 0-200 Hz to harmonize with battery testing on a test bench, based on some of the standards mentioned earlier [11].

Figure 6 illustrates a wide range of road damage, including cracked concrete, uneven roads, and potholes. These disturbances can be effectively characterized through vibration and shock testing conducted on a bench test basis. The objective is to ascertain the frequency at which the most significant magnitude is achieved.

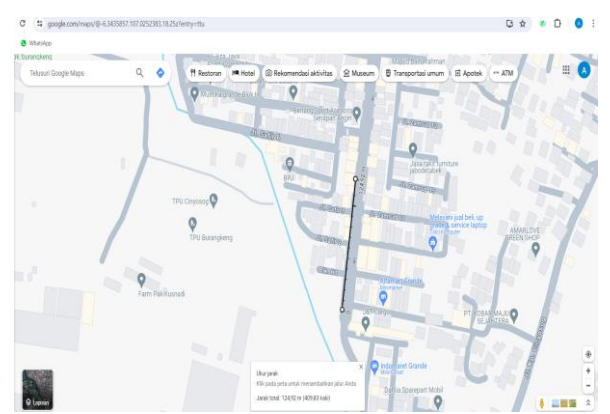
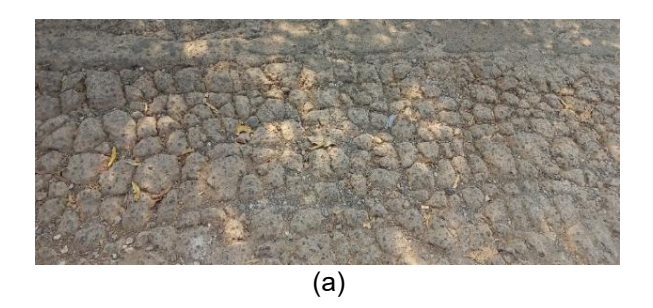
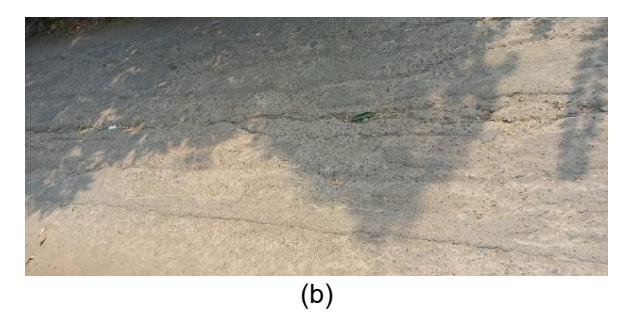


Figure 5. GPS Track Data Collection





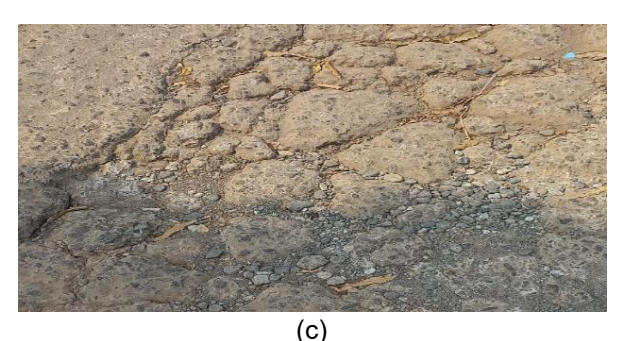


Figure 6. (a) Cracked Concrete Type Road
Damage, (b) Uneven Road Type Road Damage,
and (c) Pothole Type Road Damage

The Rion VA 12 is equipped with a data acquisition feature that facilitates direct FFT output. FFT is the result of vibration analysis viewed from a 3-dimensional perspective. Initially, the data is acquired in the time and acceleration domains. Then, using the Fourier transform, it can be presented in the frequency domain. This requires complex number analysis involving real and imaginary number components [26][27].

Figure 7 below explains how the Fourier Transform views the frequency vs amplitude plane from the side view, while the front view shows the time vs amplitude plane.

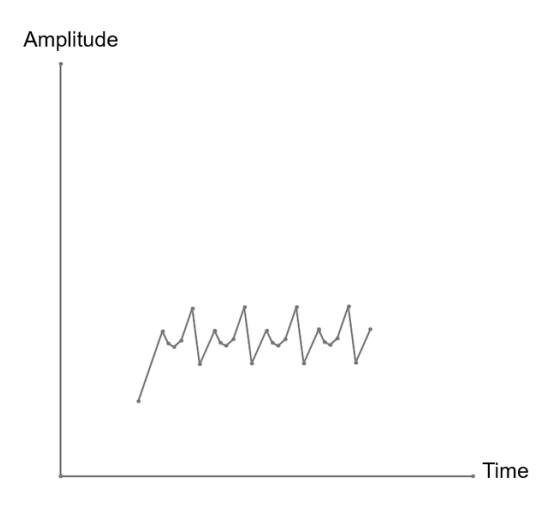


Figure 7. (a). Time Domain Original Signal

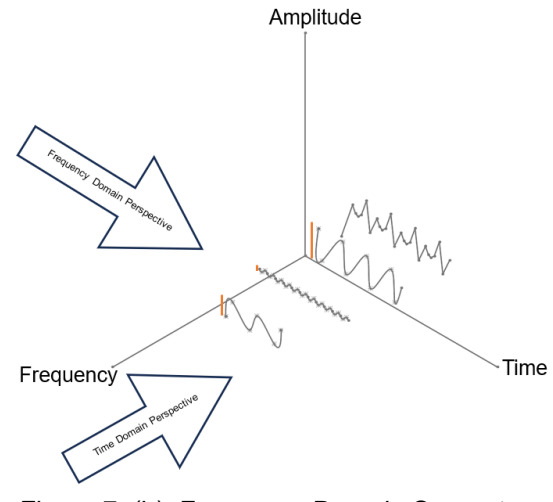


Figure 7. (b). Frequency Domain Separates Signal Into Multiple Uniform Waves.

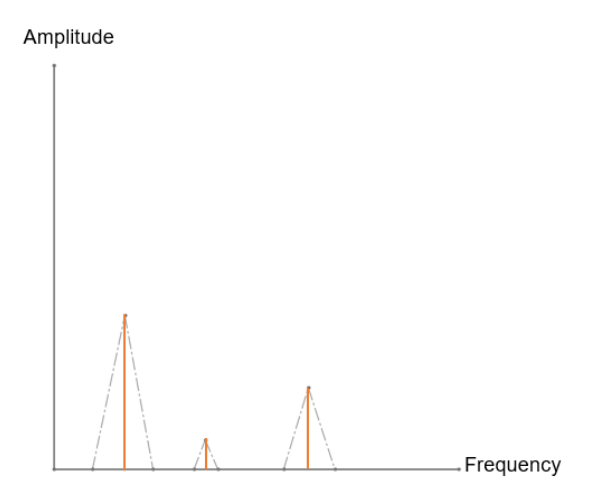


Figure 7. (c). FFT Graph Plot simplifies signal and wave problems.

As illustrated in Figure 7a, a graph of the signal function between time and amplitude is presented; however, conducting a thorough analysis of the graph is challenging. The fast Fourier transform (FFT) provides an alternative perspective, focusing on the frequency and amplitude fields depicted in Figure 7b. This approach ultimately results in Figure 7c, which offers a more accessible representation of the amplitude phenomenon that emerges at specific frequency values. This approach is instrumental in addressing diverse scenarios, including the identification of the natural frequency and the occurrence of resonance within a structure.

Researchers generally have the capacity to acquire vibration data in the time and frequency domains concurrently. However, due to the constrained capabilities of the instrument used in this study, the Rion VA 12 can only record independently in the time and frequency domains. Consequently, the present study will analyze the time domain and power spectral density obtained by transposing the graph with MATLAB. The utilization of MATLAB coding will be confined to the lowest and the highest result of the FFT graph obtained.

The following Matlab coding is employed:

```
clear
clc
fs=200:
t = 0:1/fs:1:
x=A*sin(2*pi*f*t);
y=x+randn(size(t));
subplot (3,1,1)
plot(y(1:200))
title('Noisy time domain signal')
xlabel('time t')
ylabel('Amplitude')
Y=fft(y,256);
Pvv=Y.*coni(Y)/300:
f=fs/256*(0:127);
subplot(3,1,2)
plot(f,Pyy(1:128))
title('Power Spectral Density')
xlabel('Frequency (Hz)')
subplot(3.1.3)
plot(f(1:40), Pyy(1:40))
title('Power Spectral Density')
xlabel('Frequency (Hz)')
```

Research of a similar nature employs a numerical simulation approach that utilizes fuzzy logic methods to detect imbalance and misalignment [28]. This finding underscores the value of numerical simulation in determining vibration analysis, yielding highly accurate results.

RESULTS AND DISCUSSION

After collecting data at two distinct velocities (10 km/h and 15 km/h), the experimenter conducted three replicates for each velocity. The ensuing data is presented in Figures 8 and 9.

As illustrated in Figure 8, a consistent pattern emerges across all three repetitions, with the peak FFT graph matching a frequency of 7 Hz. This frequency is accompanied by acceleration magnitude values of 1.86, 2.35, and 2.09 G, respectively, as the experiments progress from the initial to the final stage. This observation indicates that the natural frequency of the motorcycle is approximately 7 Hz.

This observation is consistent across all three repetitions. A similar trend is observed in the 15 km/h speed variation shown in Figure 9. The frequency with the highest acceleration magnitude value is again at 7 Hz, while the acceleration magnitude values are 1.79 G, 1.98 G, and 1.94 G, respectively. No significant difference is observed when comparing the results at two different speeds of 10 and 15 km/h.

However, a notable distinction emerges when comparing the 10 km/h speed to the 15 km/h speed. Specifically, the 10 km/h speed exhibits a heightened vibration disturbance compared to the 15 km/h speed. This phenomenon can be attributed to the vehicle's suspension system, which prioritizes maximizing rebound time when wheels vehicle's enter а Consequently, when exiting a pothole, the vehicle's suspension system demands a rapid compression phase, thereby contributing to the high acceleration value observed.

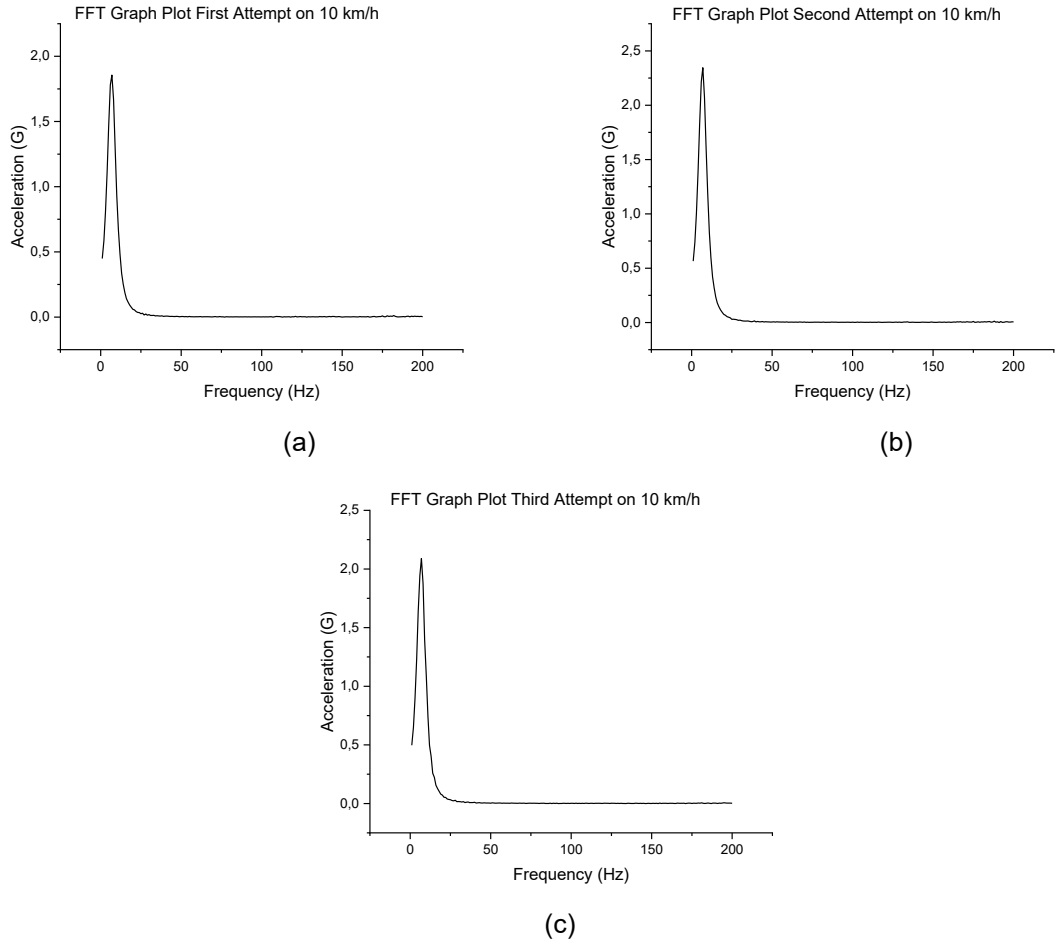


Figure 8. FFT Graph Plot on 10 km/h: (a) first attempt, (b) second attempt, and (c) third attempt

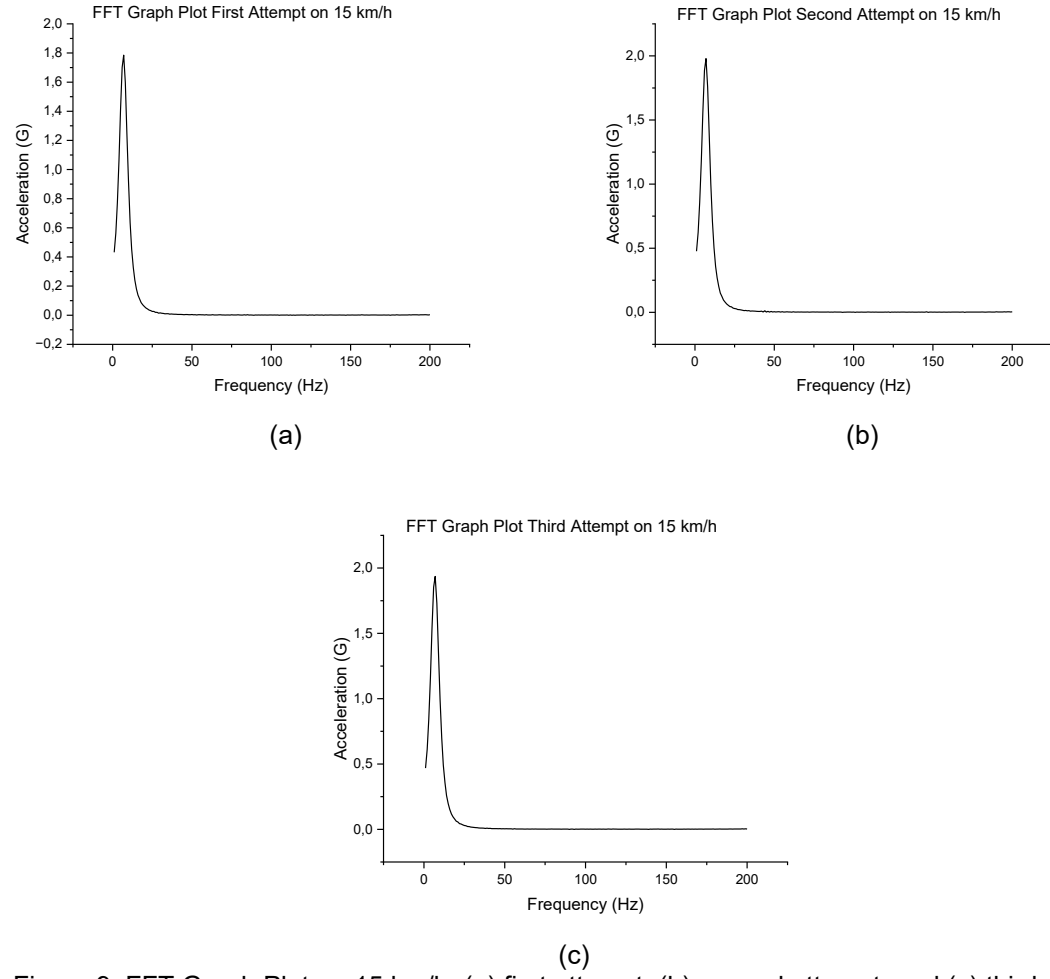


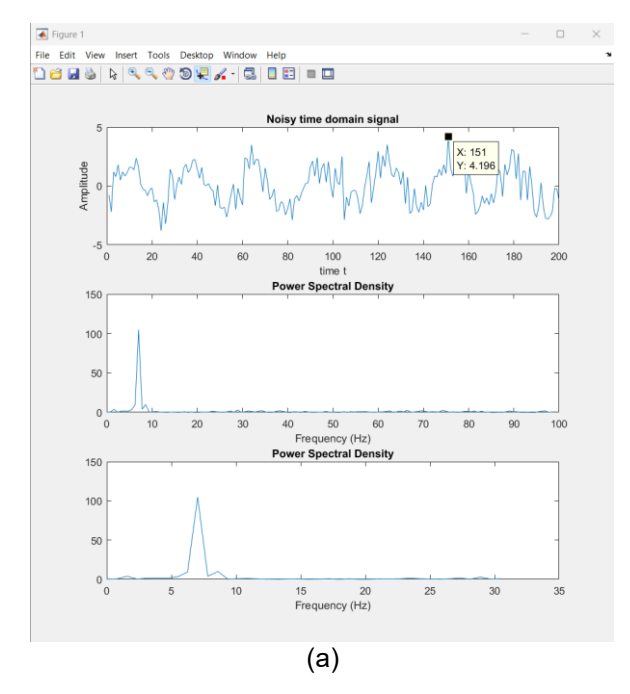
Figure 9. FFT Graph Plot on 15 km/h: (a) first attempt, (b) second attempt, and (c) third attempt

The FFT peak graph of the first experiment at 15 km/h shows the lowest FFT peak (1.79G), while the FFT peak graph of the second experiment at 10 km/h shows the highest FFT peak (2.34G). The author utilizes MATLAB coding to ascertain the time domain and PSD graph plots referenced in the method section. The ensuing results, obtained by plotting the aforementioned time domain and PSD graphs, are presented in Figure 10.

A comparison of the time domain graphs reveals that they exhibit analogous values, with seven valleys and peaks identified. The maximum values recorded were 4.196 and 4.717, respectively. However, the PSD plot indicates that the second graph exhibits twice the spectral energy density. While the FFT values of the second graph are not significantly disparate, the former exhibits a substantially higher energy density, approximately 2 times greater.

However, the second graph produces a substantially higher energy density, approximately 2 times that of the first graph. The high energy density significantly influences the acceleration of structural damage.

As previously mentioned in the method, the author selected a frequency measurement range of 0-200 Hz to analyze the discrepancy in the FFT response compared to previous research. Notably, the natural and resonant frequencies may manifest multiple times within distinct frequency ranges. However, within the 0-200 Hz range specified in this study, a solitary FFT peak was observed. However, if the frequency range is expanded, for instance, up to 2 kHz or 20 kHz, it is plausible for the FFT graph plot to manifest additional frequency peaks [26][27]. This is consistent with the augmentation in the number of tracks involved and the escalation in the velocity variations utilized.



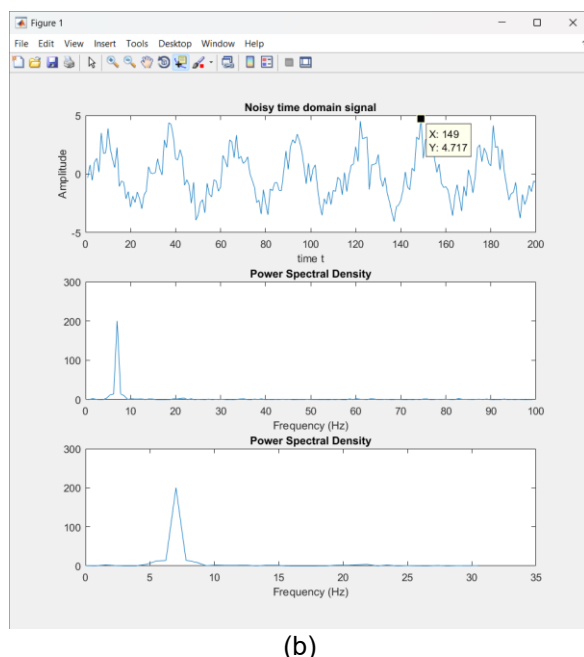


Figure 10. (a) Plot Graph Time Domain and PSD FFT = 1.79G, (b) Plot Graph Time Domain and PSD FFT = 2.34G

The FFT graph presented herein will be compared with that of previous research, which obtained the transmissibility value of a battery structure. Unlike the current research, the transmissibility value is the final result of comparing two accelerometers: one mounted on the shaker table for vibration excitation and the other on the core of the structure to be assessed for acceleration.

According to the findings of a particular study, the transmissibility of an electric vehicle battery structure has a maximum value of 1.4 at a frequency of approximately 28 Hz. The transmissibility graph is shown in Figure 11.

The transmissibility value is observed to be consistent across the second and sixth experiments, thereby validating the hypothesis that the natural frequency of REESS is 28 Hz. Regarding the FFT increments and peaks, the frequency range, spanning from 0 to 200 Hz, exhibits a similarity in which the peak of the FFT graph manifests once.

The method used in the extant study was also employed in another study, which posits that an accelerometer is installed on the vehicle knuckle (unsprung mass) to detect cracks or other damage on a road track. The results of the study are shown in Figure 12.

The present research method involves installing accelerometers within the sprung mass area to determine the natural frequency of the vehicle system, which includes springs, dampers, and additional suspension components such as swing arms [29, 30, 31].

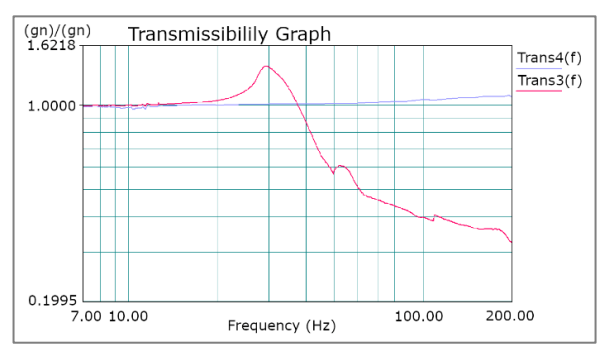


Figure 11. Transmisibility Graph Plot for REESS Vibration Testing

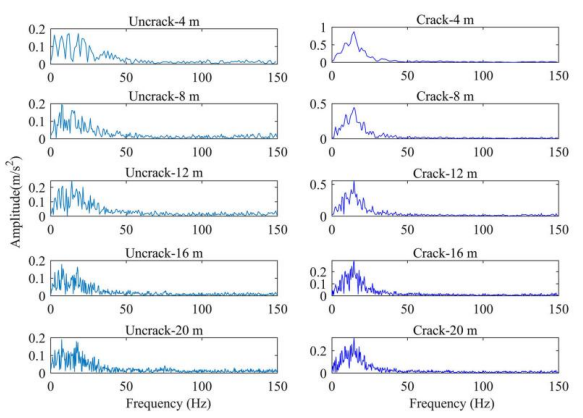


Figure 12. Acceleration Magnitude Track
Distance Domain [29]

Another study evaluated the extent of damage to a vehicle's shock absorber. This assessment involved the installation of accelerometers on the shock absorber [32].

FFT analysis has been demonstrated to offer significant advantages across a range of disciplines, particularly in the domain of vehicle vibration knowledge. The installation methods of accelerometers, which measure vibrations, vary depending on the purpose. Some are installed in unsprung mass areas, such as knuckles and axles, while others are installed in sprung mass areas, such as cabin and seat areas, to determine passenger comfort. Some are installed in the chassis area to determine the natural frequency, while others are placed in the shock absorber mounting area to assess the level of shock absorber damage. Existina research characterizes vehicle vibrations in the battery pack or REESS. In the future, developing a REESS support system is anticipated to minimize the acceleration level on the FFT plot, thereby ensuring more robust battery pack protection.

CONCLUSION

Vibration is an inherent and inevitable mechanical phenomenon. At elevated levels, this phenomenon can inflict harm upon structures. As outlined in numerous standards, vibration testing is mandatory for electric vehicle batteries. Vibration testing is a crucial component of ensuring the mechanical integrity of these batteries. This research focuses on a novel approach to vibration testing: conducting tests directly on the road. The highest FFT value recorded was at 2.35 G. Previous studies have explored related topics. FFT analysis with accelerometer installation offers numerous benefits, such as assessing component damage, determining passenger comfort, and acquiring road damage data, considering variations in accelerometer installation on sprung unsprung mass. In the future, improvements can be made to the battery support structure to achieve a higher level of safety, indicated by a decrease in the peak value of the FFT.

ACKNOWLEDGMENT

The MAF would like to express its gratitude to the Head of VTCC for kindly allowing the utilization of the portable vibration analyzer.

CONTRIBUTION

MAF is responsible for the research design, data collection, and conceptualization. IST is tasked with writing and revising the article. DF, HF,

and HP supervise the research. The authors have thoroughly reviewed the final article and have consented to its publication.

REFERENCES

- [1] N. P. Chavan, M. S. Kale, S. P. Deshmukh, and C. M. Thakar, "A Review on Development and Trend of Condition Monitoring and Fault Diagnosis," ECS Transactions (ECST), vol. 107, no. 1, p. 17863, Apr. 2022, doi: 10.1149/10701.17863ecst.
- [2] K. Ikeda et al., "Vibration Characteristics Control of Resonance Point in Vehicle: Fundamental Considerations of Control System without Displacement and Velocity Information," Vibration, vol. 6, no. 1, pp. 1–10, Mar. 2023, doi: 10.3390/vibration6010001.
- [3] Y. Qin et al., "Noise and vibration suppression in hybrid electric vehicles: State of the art and challenges," Renewable and Sustainable Energy Reviews, vol. 124, no. February, p. 109782, 2020, doi: 10.1016/j.rser.2020.109782.
- [4] R. Han, "Implementation of Fast Fourier Transform in image processing, signal processing and acoustics," *IET Conference Proceedings*, vol. 2024, no. 24, pp. 450–455, 2025, doi: 10.1049/icp.2024.4549.
- [5] S. Kawakami and D. Takahashi, "Implementation and Evaluation of Octuple-Precision Fast Fourier Transform on GPU," in 2024 IEEE International Symposium on Parallel and Distributed Processing with Applications (ISPA), 2024, pp. 287–294. doi: 10.1109/ISPA63168.2024.00044.
- [6] A. Byou, A. Derouich, A. Saadi, M. Said, E. Houssam, and E. idrissi Abderrahman, "Early Detection of Mechanical Faults in Loads Coupled with Asynchronous Electric Motor," in *Digital Technologies and Applications*, S. Motahhir and B. Bossoufi, Eds., Cham: Springer Nature Switzerland, 2024, pp. 424–433.
- [7] U. Awan, K. Ghabraie, A. Zolfagharian, and B. Rolfe, "Impact of vibrations on lithium-ion batteries in electric vehicles: sources, degradation mechanisms, and testing standards Impact of vibrations on lithium-ion batteries in electric vehicles: sources, degradation mechanisms, and testing standards," *Journal of Physics-Energy*, vol. 7, p. 022003, 2025.
- [8] P. Berg et al., "Durability of lithium-ion 18650 cells under random vibration load with respect to the inner cell design," Journal of Energy Storage, vol. 31, 2020, doi:

- 10.1016/j.est.2020.101499.
- [9] Z. B. Omariba, L. Zhang, H. Kang, and D. Sun, "Parameter identification and state estimation of lithium-ion batteries for electric vehicles with vibration and temperature dynamics," World Electric Vehicle Journal, vol. 11, no. 3, 2020, doi: 10.3390/WEVJ11030050.
- [10] K. Shukla, A. R. M. Siddique, K. Venkateshwar, M. R. Mohaghegh, S. H. Tasnim, and S. Mahmud, "Experimental investigation on thermal field measurement of lithium-ion batteries under vibration," *Journal of Energy Storage*, vol. 53, p. 105110, 2022, doi: https://doi.org/10.1016/j.est.2022.105110.
- [11] M. A. Firmansyah, N. Ruhyat, and H. Firdaus, "Influences of Vibration Exposure on Battery Pack for Two- Wheeler Electric Vehicles," *Evergreen*, vol. 11, no. 03, pp. 2700–2710, 2024.
- [12] T. You, J. Zhou, D. Gong, Y. Sun, B. Li, and J. Chen, "Synthesis of random vibration environment spectra for the fatigue analysis and optimization of railway vehicles," *International Journal of Fatigue*, vol. 159, no. September 2021, p. 106752, 2022, doi: 10.1016/j.ijfatigue.2022.106752.
- [13] J. Qian, Y. Cen, X. Pan, Y. Tian, and S. Liu, "Spectrum parameters for runway roughness based on statistical and vibration analysis," *International Journal of Pavement Engineering*, vol. 23, no. 11, pp. 3757–3769, 2021, doi: 10.1080/10298436.2021.1916821.
- [14] P. Múčka, G. J. Stein, and P. Tobolka, "Whole-body vibration and vertical road profile displacement power spectral density," *Vehicle System Dynamics*, vol. 58, no. 4, pp. 630–656, 2020, doi: 10.1080/00423114. 2019.1595675.
- [15] W. Yin and Y. Qiu, "Comparison of the vertical transmissibility of the suspension seat under single-axis vertical vibration and tri-axis vibration: Effect of the magnitude of in-line vertical and horizontal vibration," in "Advances in Acoustics, Noise and Vibration 2021" Proceedings of the 27th International Congress on Sound and Vibration, ICSV 2021, 2021.
- [16] W. Yin and Y. Qiu, "An experimental study of the vertical transmissibility of the suspension seat with tri-axis translational vibration," *Shengxue Xuebao/Acta Acust.*, vol. 49, no. 2, pp. 209 – 216, 2024, doi: 10.12395/0371-0025.2023191.
- [17] B. B. Mandal, A. Bhattacharjee, S. Prajapati,

- and S. A. Hussain, "A comparative study of transmissibility factors of traditional and pneumatic dumper seats using one-third octave band analysis," *Noise & Vibration Worldwide*, 2020, doi: 10.1177/0957456520924816.
- [18] G. Priyandoko, P. Suwandono, M. I. N. Sasongko, Ubaidillah, and S. T. Wicaksono, "Developing adjustable stiffness for smart material of magnetorheological elastomer to diminish vibration," *Sinergi (Indonesia)*, vol. 28, no. 1, pp. 163–168, 2024, doi: 10.22441/sinergi.2024.1.016.
- [19] C. Deng, Q. Deng, W. Liu, C. Yu, J. Hu, and X. Li, "Analysis of vibration and noise for the powertrain system of electric vehicles under speed-varying operating conditions," *Mathematical Problems in Engineering*, vol. 2020, 2020, doi: 10.1155/2020/6617291.
- [20] P. Charoen-amornkitt, K. Nantasaksiri, K. Ruangjirakit, and Y. Laoonual, "Energy consumption and carbon emission assessment of battery swapping systems for electric motorcycle," *Heliyon*, vol. 9, no. 12, p. e22887, 2023, doi: 10.1016/j.heliyon.2023. e22887.
- [21] P. Kushare, P. Pillai, and A. Pelagade, "Design and optimization of the electric motorcycle chassis for effective battery swapping," *AIP Conf. Proc.*, vol. 3111, no. 1, p. 40005, Jul. 2024, doi: 10.1063/5.0221414.
- [22] S. Hussain, W. A. W. Ghopa, S. S. K. Singh, A. H. Azman, and S. Abdullah, "Experimental and Numerical Vibration Analysis of Octet-Truss-Lattice-Based Gas Turbine Blades," *Metals (Basel).*, vol. 12, no. 2, 2022, doi: 10.3390/met12020340.
- [23] F. Viswambharan and S. K. C. P., "Effects of mass and sitting posture of tractor operators on the vibration transmissibility," SSRN Electron. J., pp. 392–397, 2021, doi: 10.2139/ssrn.3794641.
- [24] M. Frydrysiak and Z. Pawliczak, "Design and Testing of 3D Textile Materials with Vibro-Insulating Properties, Applicable in the Construction of Vibroisolating Seats for Machine and Device Operators," *Fibres Text. East. Eur.*, vol. 32, no. 3, pp. 57–68, 2024, doi: 10.2478/ftee-2024-0020.
- [25] M. Jomoto and A. Kawamura, "Study on Relationship Between Road Profile and Structural Damage of the Pavement," in Advances in Environmental Vibration and Transportation Geodynamics II, T. Ishikawa, E. Tutumluer, and S. Miyamoto, Eds., Singapore: Springer Nature Singapore, 2025,

- pp. 247-260.
- [26] Y. Wang, "Vibration Signal Extraction Based on FFT and Least Square Method," *IEEE*, vol. 8, 2020, doi: 10.1109/ACCESS.2020. 3044149.
- [27] S. Das, A. Saha, and C. S. Kumar, "Calibrated non-contact vibrational harmonics measurement based on selfvibration compensated 2D-PSD with MEMS accelerometer using FFT analysis," *IET Sci. Meas. Technol.*, vol. 14, no. 8, pp. 877–882, 2020, doi: 10.1049/iet-smt.2019.0229.
- [28] D. Romahadi, D. Feriyanto, F. Anggara, F. P. Wijaya, and W. Dong, "Intelligent system design for identification of unbalance and misalignment using Fuzzy Logic methods," *Sinergi (Indonesia)*, vol. 28, no. 2, pp. 241–250, 2024, doi: 10.22441/sinergi.2024.2.004.
- [29] A. Čerškus, T. Lenkutis, N. Šešok, A. Dzedzickis, D. Viržonis, and V. Bučinskas, "Identification of road profile parameters from vehicle suspension dynamics for control of damping," Symmetry (Basel)., vol. 13, no. 7,

- 2021, doi: 10.3390/sym13071149.
- [30] Q. Yang and S. Zhou, "Identification of asphalt pavement transverse cracking based on vehicle vibration signal analysis," *Road Mater. Pavement Des.*, vol. 22, no. 8, pp. 1780–1798, 2021, doi: 10.1080/14680629.2020.1714699.
- [31] E. D. Dimaunahan, K. A. P. Abo, C. D. Ricafort, X. R. Gabayeron, and L. M. L. Teope, "Road Surface Quality Assessment Using Fast-Fourier Transform," 2020 IEEE 12th Int. Conf. Humanoid, Nanotechnology, Inf. Technol. Commun. Control. Environ. Manag. HNICEM 2020, 2020, doi: 10.1109/HNICEM51456.2020.9399996.
- [32] R. Burdzik, "A comprehensive diagnostic system for vehicle suspensions based on a neural classifier and wavelet resonance estimators," *Measurement*, vol. 200, no. February, p. 111602, 2022, doi: 10.1016/j.measurement.2022.111602.